A sampling-based path planning algorithm for improving observations in tropical cyclones

Justice Darko[1], Larkin Folsom[1], Hyoshin Park[1], Masashi Minamide[2], Masahiro Ono[3], and Hui Su[4]

[1]North Carolina Agricultural and Technical State University
[2]The University of Tokyo
[3]NASA Jet Propulsion Laboratory
[4]Jet Propulsion Laboratory, California Institute of Technology

November 23, 2022

Abstract

Lack of high-resolution observations at the inner-core region of tropical cyclones introduces uncertainty into the structure's true initial state. More accurate measurements at the inner-core are essential for accurate tropical cyclone forecasts. This study seeks to improve the estimates of the inner-core structure by utilizing *background* information from prior assimilated conventional observations. We provide a scheme for targeted high-resolution observations for platforms such as the Coyote sUAS. In an effort to identify potential locations of high uncertainty, an exploratory investigation of the *background* information of the state variables pressure, temperature, wind speed, and a combined representation of the state variables given by their linear weighted average is presented. A sampling-based path planning algorithm that considers the Coyote's energy usage then locates the regions of high uncertainties along a Coyote's flight, allowing us to maximize the removal of uncertainties. The results of a data assimilation analysis of a typical Coyote flight mission using the proposed deployment scheme shows significant improvements in estimates of the tropical cyclone structure after the resolution of uncertainties at targeted locations.

A sampling-based path planning algorithm for improving observations in tropical cyclones.

Justice Darko[1], Larkin Folsom[1], Hyoshin Park[1], Masashi Minamide[2], Masahiro Ono[3], Hui Su[3]

[1]Department of Computational Science & Engineering
North Carolina A&T State University
1601 E. Market Street
Greensboro, NC 27411
[2]Department of Civil Engineering
The University of Tokyo
7-3-1 Hongo, Bunkyo-ku
Tokyo, 113-8656, Japan
[3]NASA Jet Propulsion Laboratory
M/S 183-701
4800 Oak Grove Drive
Pasadena, CA 91109

Key Points:

- A novel implementation of a sampling-based path planning algorithm in TC space.
- Coyote sUAS navigation in TCs to maximize the removal of uncertainty from start to goal location.
- Evaluation based on prior estimates of TC uncertainty distribution from state-of-the-art assimilation system.

Corresponding author: Justice Darko, `jdarko@aggies.ncat.edu`

Abstract

Lack of high-resolution observations at the inner-core region of tropical cyclones introduces uncertainty into the structure's true initial state. More accurate measurements at the inner-core are essential for accurate tropical cyclone forecasts. This study seeks to improve the estimates of the inner-core structure by utilizing *background* information from prior assimilated conventional observations. We provide a scheme for targeted high-resolution observations for platforms such as the Coyote sUAS. In an effort to identify potential locations of high uncertainty, an exploratory investigation of the *background* information of the state variables pressure, temperature, wind speed, and a combined representation of the state variables given by their linear weighted average is presented. A sampling-based path planning algorithm that considers the Coyote's energy usage then locates the regions of high uncertainties along a Coyote's flight, allowing us to maximize the removal of uncertainties. The results of a data assimilation analysis of a typical Coyote flight mission using the proposed deployment scheme shows significant improvements in estimates of the tropical cyclone structure after the resolution of uncertainties at targeted locations.

1 Introduction

Understanding the fundamental role of the boundary layer (i.e., interface between the ocean and atmosphere) of tropical cyclones (TCs) plays a significant role in providing essential meteorological information. The boundary layer contains important information about the inner core dynamics and requires a true and thorough examination to predict the track and intensity of TCs. An undesirable phenomenon such as rapid intensification, which describes how TCs can increase in intensity over short periods, can be accurately predicted from an observation of the boundary layer (Cione et al., 2013). In recent studies, inner-core observations have been done with next-generation weather satellites (F. Zhang et al., 2019). Nonetheless, targeted high-resolution observations using platforms such as small Unmanned Aircraft System (sUAS) can significantly improve information (Pillar-Little et al., 2020) about the inner-core and eventually improve TC estimates for forecast models.

The Coyote program (Cione et al., 2016; de Boer et al., 2019), introduced by the national hurricane center by NOAA's air reconnaissance programs, well supports the task of monitoring targeted critical layers of a TC. The Coyote program allows the sUAS to be deployed to the low altitude boundary layer, which is extremely dangerous for manned in-situ measurements. However, the Coyote program has several limitations that can be significantly improved by the proposed deployment method. First, the Coyote program has focused on successfully collecting data with drone flight patterns (e.g., eyewall and inflow module) conceived from procedures described in NOAA's Hurricane Research Division Annual Hurricane Field Program. However, these predefined navigation procedures do not necessarily consider how data gathered from a flight path impacts and improves the posterior estimate of the TC at a future time from an earlier prior estimate of the TC. The criteria for location selection was "*difficult to observe in sufficient detail*" in the eye which is the most recognizable feature of the TC spanning between 20-50 km in diameter, rather than "*importance of information*" gained from the data in a smaller, more precise target location. A Coyote sUAS with its limited endurance and range must consider how traversing a given path, or flight pattern will maximize the resolution of uncertainties in previous TC estimates. For example, in a study by F. Zhang et al. (2019), uncertainties for state variables are estimated from the assimilation of conventional in situ data and Geostationary Operational Environmental Satellite (GOES)-All-Sky Radiances. These uncertainties can provide background information for targeted high-resolution observations to maximize the removal of uncertainties in the prior estimates of the TC, providing a more accurate approximation for forecast models.

Second, current Coyote flight navigation does not explicitly consider how the path affects the limited battery life (critical for observations and communication) and total distance covered by the Coyote. For instance, flying at certain angles to the direction of the TC wind velocity will severely impact battery usage. A flight pattern that strives to reduce the energy utilized for navigation will improve the range for observations. The current study seeks to reduce the energy utilized for navigation and improve the distance covered by the sUAS by flying as close as possible with the drift of TC winds. To the best of our knowledge, this is the first study that uses a sampling-based planning algorithm to locate regions of high uncertainties for Coyote sUAS along a path to a target location, and overall, improve the efficiency of Coyote battery usage.

2 Related Work

Several environmental and storm-related factors have been studied to understand the combined impacts on the future structure of TCs. Humidity, absolute vorticity, and distribution of convection relative to the storm are observed to affect TCs intensification (Munsell et al., 2013; Sippel & Zhang, 2008, 2010). A strong relationship has been observed between the measurement of the central pressure of TC, and its maximum sustained winds speed (Rosendal & Shaw, 1982). The sensitivity of predictive models of TCs to high-resolution atmospheric data is currently receiving significant attention (Raavi & Walsh, 2020).

Table 1. Summary of TC Prediction Parameters of Interest

Parameters	**Target**	**Observational Equipment**	**Forecast**	**Previous studies (Examples)**
Wind speed, Wind Direction	Eye, Eyewall, inflow, PBL	Reconnaissance aircrafts (> 2 km), Buoys (SST), UAS (< 2km), Dropsonde	Intensity, Structure	Rosendal and Shaw (1982), Cione et al. (2020), Stern et al. (2016), DeMaria and Kaplan (1999), DeMaria et al. (2005, 2014)
Air Temperature, SST*	PBL, Inflow, Upper-Ocean Layers		Intensity, Structure, Track	Sanabia et al. (2013), J. A. Zhang et al. (2017), Cione et al. (2020), Stern et al. (2016), DeMaria and Kaplan (1999), DeMaria et al. (2005, 2014)
Pressure	Eye, Eyewall, Inflow, PBL	Reconnaissance Aircrafts (> 2 km), UAS (< 2km), Dropsonde		Rosendal and Shaw (1982), Goyal and Datta (2011), J. A. Zhang et al. (2017), Cione et al. (2020), Stern et al. (2016), DeMaria and Kaplan (1999), DeMaria et al. (2005, 2014)
Moisture (RH*)	Eyewall, Inflow, PBL		Intensity, Structure	Sippel and Zhang (2008, 2010), Munsell et al. (2013), Van Sang et al. (2008), J. A. Zhang et al. (2017), Cione et al. (2020), Stern et al. (2016), DeMaria and Kaplan (1999), DeMaria et al. (2005, 2014)
TKE Momentum Flux	Eyewall, Inflow, PBL (< 150m)	UAS (< 2km) Dropsondes	Intensity, Structure	Cione et al. (2020), Stern et al. (2016), Pillar-Little et al. (2020)

*SST: sea surface temeperature; RH: relative humidity; PBL: planetary boundary layer.

The impact of data assimilation analysis for identifying the role of internal dynamics on intensification and structural changes in TCs revealed that hybrid data assimilation techniques improved the overall quality of prediction compared to individual data assimilation methods (Malakar et al., 2020). A flow-dependent sequential assimilation-based targeted observation has been developed using the ensemble Kalman filter to minimize the analysis error variance (Wu et al., 2020). Data assimilation experiments by Cione et al. (2020) show how sUAS data can be used to improve storm structure analysis. A review of continuous monitoring of a TCs' core using sUAS is provided in Tyrrell and Holland (2003). Aircraft observations of upper-ocean thermal structures show that there is a strong correlation between the upper-ocean thermal variability and the intensity change of TCs (Sanabia et al., 2013). Prediction accuracy of TCs in both coupled dynamical and statistical models was improved by successful observation and assimilation of upper ocean temperature (Sanabia et al., 2013). Table 1 summarizes some common observational parameters that are collected for the estimates of a TC structure required for an accurate TC forecast.

The remainder of this paper's structure is as follows: section 3 describes the sampling-based method, development of a combined measure of uncertainty, and a presentation of a constraint for safe and energy-efficient navigation. In section 4, we present an evaluation of the model performance and test its robustness through a Monte-Carlo simulation. Section 5 presents an illustration of a typical Coyote sUAS mission utilizing the proposed deployment scheme, with data assimilation analysis to estimate improvement levels. Finally, a summary of the study's findings and future research direction is presented in section 6.

3 Model, Data, and Methods

The highly dynamic environment of a TC configuration space is mainly described through the wind velocities. To provide easy maneuverability for Coyote sUAS in such environments, a rapidly exploring random tree star (RRT*) algorithm which converges to a collision-free path presents an appealing approach for an efficient path solution. RRT* algorithm starts with a tree that includes the initial drop off location of the Coyote as its single vertex and no edges. The algorithm then incrementally grows a tree on the TC configuration space by randomly sampling a location within the space and extending it towards that location. This study uses the RRT* algorithm to model the Coyotes' flight for targeted observations. The observations are characterized by the uncertainty distribution of three state variables, namely pressure, temperature, and wind speed (mainly because of the current capabilities of the Coyote sUAS). Based on the aforementioned state variable uncertainties, a combined representation of the uncertainties at different locations in the TC configuration space is developed through a linear weighted average of the three individual uncertainty distributions. The combined representation for uncertainty $\hat{C}_i$ at location i in the TC 's configuration space is therefore written as:

$$\hat{C}_i = W_P \hat{x}_i^P + W_T \hat{x}_i^T + W_W \hat{x}_i^W, \tag{1}$$

where $\hat{x}_i^P, \hat{x}_i^T, \hat{x}_i^W$, are the normalized uncertainties for pressure, temperature, and wind speed uncertainty, and W_P, W_T, W_W, are the weights for pressure, temperature, and wind speed uncertainty. The normalized uncertainties for each state variable x_i at location i is written as:

$$\hat{x}_i = \frac{x_i - x_{\min}}{x_{\max} - x_{\min}}, \tag{2}$$

where $x_{\min}$ and $x_{\max}$ are minimum and maximum uncertainty for the given state variable. The weights for the state variable uncertainty sums to one, written as:

$$W_P + W_T + W_W = 1. \tag{3}$$

3.1 TC STRAP-RRT*.

Suas naviga**T**ion with en-**R**oute measurement **A**ccumulation **P**lan (STRAP) is developed as an extension of the RRT* algorithm. The main objective is to find random nodes that lower the overall energy for a given path but maximizes the uncertainty removed along the path to a target location. In order to guarantee minimal energy is utilized for navigation, a wind velocity constraint is implemented as the acceptable angular difference between a sub-path segment of the RRT* tree and the wind direction at location i. For this study, the angular difference condition is set at less or equal to 50^o (allowing some room to navigate around the direction of the wind). The set of all the configurations satisfying the wind velocity constraints is written as:

$$H_{con} = \{q : f_i(q) \leq \epsilon_i\}, \epsilon_i \in [0; 50), \forall i \geq 0 \tag{4}$$

H_{con} is TC configuration space and $f_i(q)$ is written as:

$$f_i(q) = \cos\alpha = \frac{\bar{a_i} \cdot \bar{b_i}}{|\bar{a_i}| \cdot |\bar{b_i}|}, \tag{5}$$

where $\bar{a_i}$ and $\bar{b_i}$ are the TC wind and RRT* branch at location i.

An end result of the wind velocity constraint is an increased range of coverage by the Coyote sUAS for the same endurance. The speed of the Coyote sUAS relative to a fixed point on the earth's surface (ocean) is the ground speed (Figure 1).

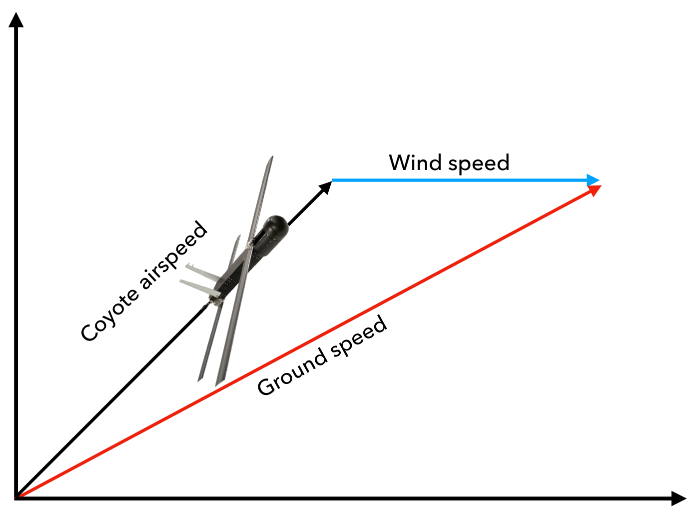

Figure 1. Coyote ground speed representation.

The velocity of the Coyote sUAS is thus given as the vector sum of the Coyote airspeed and the TC wind speed, written as:

$$\bar{V}_{Ground} = \bar{V}_{Coyote} + \bar{V}_{Wind} \tag{6}$$

It can be seen from Equation 6 that the relative speed of the Coyote sUAS to the ocean is more than the Coyote airspeed. This important deduction is developed as a result of the wind velocity constraint. For example, in a scenario where the angular difference between the Coyote and wind speed is zero, the speed of the Coyote relative to the ocean will be the sum of the TC wind and Coyote's speed.

For an illustration of STRAP-RRT* algorithm (Figure 2), we first extend a nearest-neighbor vertex towards a randomly sampled location in the TC configuration space. The extension process creates a new vertex q_{new}, at a distance $\leq$ to a defined step size. The algorithm then connects q_{new}, to the vertex that incurs the maximum total uncertainty ($\sum M_{unc}$) from our start location within the set of vertices found in a defined vicinity around q_{new} (parent stage). STRAP-RRT* also reevaluates previous connections and extends the new vertex to the vertex that can be accessed through the maximum uncertainty, described as the rewire stage. At the point of rewiring, the algorithm searches among all existing nodes within the defined vicinity of q_{new}.

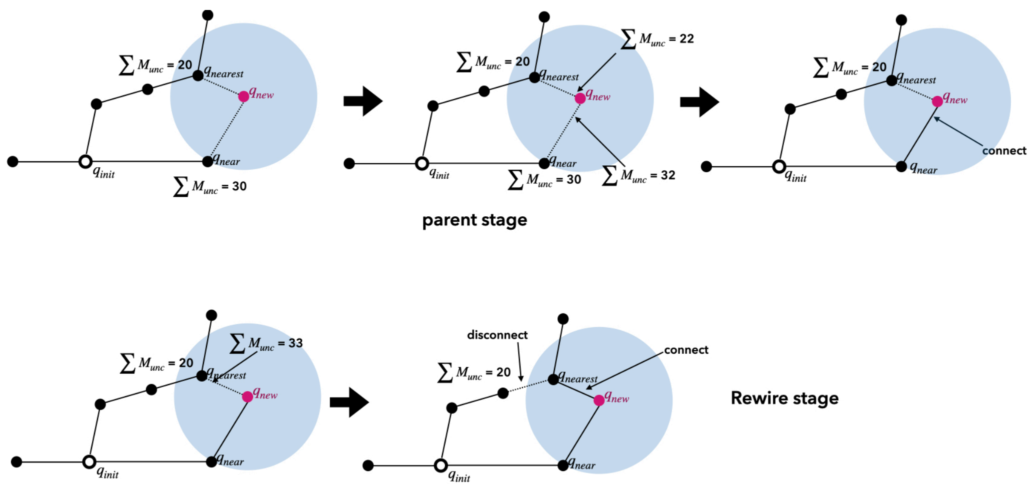

Figure 2. Stages of RRT* for exploring TC space.

As shown in the pseudocode (Algorithm 1), the `Nearest` function in STRAP-RRT* (`NearestSTRAP`) considers the uncertainty at the nearest node. `NoExceed` conditional statement implements the wind velocity constraint. The `ChooseParent` function considers the closest node by uncertainty, rather than distance.

Algorithm 1 : STRAP-RRT*

T ← InitializeTree()
T ← InsertNode($\emptyset$,z_{init},T)
for i=0 to i=N **do**
  z_{rand} ← Sample(i)
  $z_{nearest}$ ← NearestSTRAP(T,z_{rand})
  (z_{new}, U_{new}) ← Steer$(z_{nearest}, z_{rand})$
  if NoExceed(z_{new}) **then**
    z_{near} ← Near$(T, z_{new}, |V|)$
    z_{max} ← ChooseParentSTRAP$(z_{near}, z_{nearest}, z_{new})$
    T ← InsertNode(z_{max}, z_{new}, T)
    T ← Rewire$(T, z_{near}, z_{max}, z_{new})$
  end if
end for

4 Model Evaluation

This section provides an evaluation of the model for different random scenarios. The analysis of uncertainty distribution for thermodynamic (pressure and temperature) and kinematic (wind speed) observations is performed using the modified sampling-based planning algorithm STRAP-RRT*. We compare this to a benchmark approach, the minimum distance method (MDM) subject to the wind velocity constraint.

As demonstrated by Cione et al. (2020), Coyote sUAS observations are usually done at a constant altitude, thus we assume a level flight for Coyote in situ observations. A typical Coyote sUAS battery life supports 3600s endurance, shorter if in a highly turbulent environment. At a maximum cruising airspeed of 36 ms^{-1} (Cione et al., 2016), the total distance that can be covered by Coyote sUAS assuming battery life of 3600s is 80 miles. This distance is significantly increased when the wind velocity constraint is factored. To transmit data in near-real time during observations, Coyote sUAS are equipped with a 350-MHz data link that improves the communication range of the Coyote substantially and allows the P-3 hurricane hunter aircraft to execute normal flight paths while Coyote sUAS navigates its path.

4.1 Preliminary Analysis of Uncertainty Distribution

The background information utilized in this study is developed and presented by F. Zhang et al. (2019); Minamide et al. (2020). This dataset is generated for Hurricane Harvey from the state-of-the-art data assimilation system known as the ensemble Kalman filter (EnKF) hurricane analysis and forecast system, developed at the Pennsylvania State University, which is built around the Advanced Weather Research and Forecasting Model (WRF-ARW) and the Community Radiative Transfer Model (CRTM). The data assimilation process uses conventional in-situ observations and all-sky satellite radiance from GOES-16, and produces prior estimates of the TC with an hourly temporal resolution. In this study, we assume a fixed time window for the background information based on the hourly temporal resolution. Figure 3 shows the contour plots of uncertainty distributions (estimated standard deviation) for pressure (Figure 3a), temperature (Figure 3b), wind speed (Figure 3c), and the combined representation using Equation 1 (Figure 3d) at an altitude of 1.1 km above sea level (ASL).

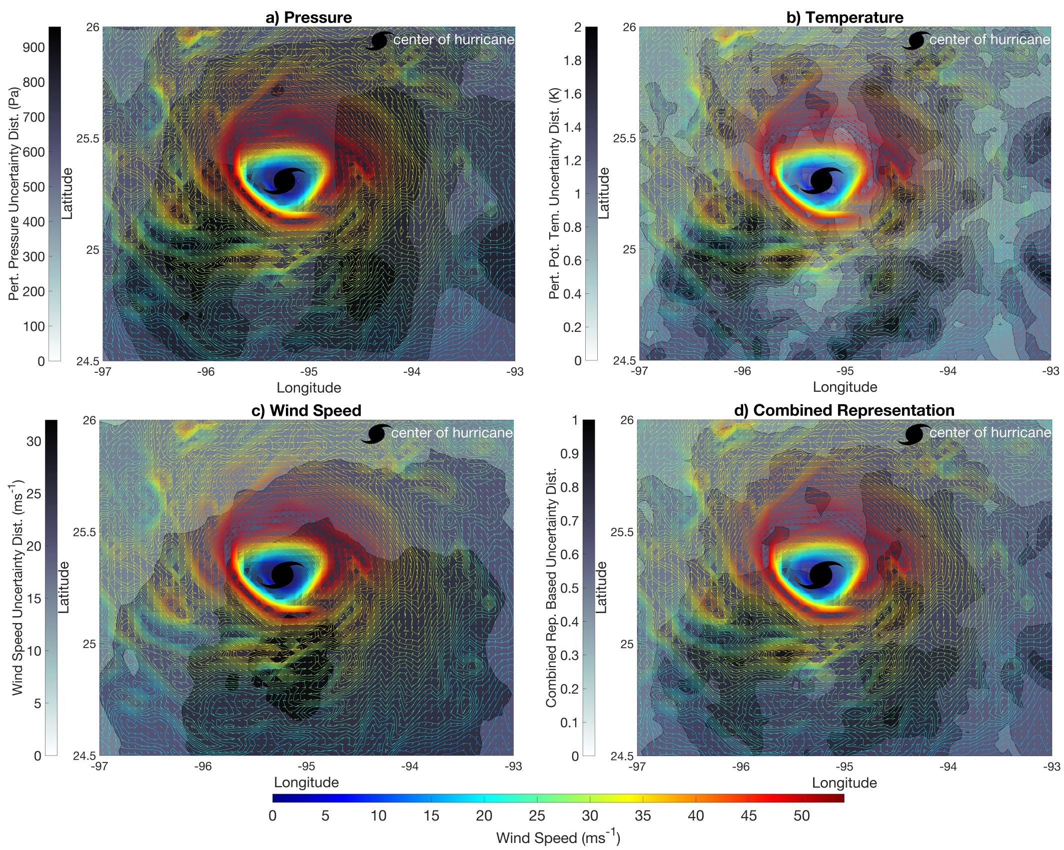

Figure 3. Uncertainty distribution for state variables at an altitude 1.1 km (ASL) for Hurricane Harvey overlaid with wind speeds on 25th August 2017, TIME: 00:00:00.

The contour plots show different degrees of uncertainties at different locations of the hurricane configuration space. Each plot of uncertainty distribution is overlaid with the hurricane's wind speed distribution to show important storm regions such as the eyewall. As shown in Figure 3, a mostly homogeneous and regular pattern is observed for pressure and wind speed uncertainty estimates. This similarity may be due to the previously observed correlation between pressure and wind speed, presented by Rosendal and Shaw (1982). Although temperature uncertainties exhibited an irregular pattern, the uncertainties for the combined representation is seen to follow the regular patterns of pressure and wind speed. By using the knowledge of the background uncertainties of the prior TC estimates, the accuracy of a posterior estimate of the TC can be improved by targeting the locations of high uncertainties.

4.2 Model Performance

The simulation results for STRAP-RRT* and MDM are first reported for a random start and goal location in the hurricane's inner-core region (within a radius of 57.539 miles from the center of the storm (Shea & Gray, 1973)). Several studies (Cione et al., 2013, 2016) have reported this region to provide meaningful data for forecasting the intensity and track of hurricanes. The Coyote start location is at 25.23^o N, 94.65^o W, and the goal location is at 25.54^o N, 94.71^o W. Figure 4 shows the tree structure and the Coyote path solutions for STRAP-RRT* and MDM overlaid on the uncertainty distribution plots. Comparing the same number of observation points in each scenario, the path solution for STRAP-RRT* showed considerable potential in improving pressure observations by selecting points of high-pressure uncertainties (Figure 4a). Specifically, the total uncertainty removed by STRAP-RRT* and MDM are 10751 Pa and 5917.7 Pa respectively, which corresponds to improvement of over 81%.

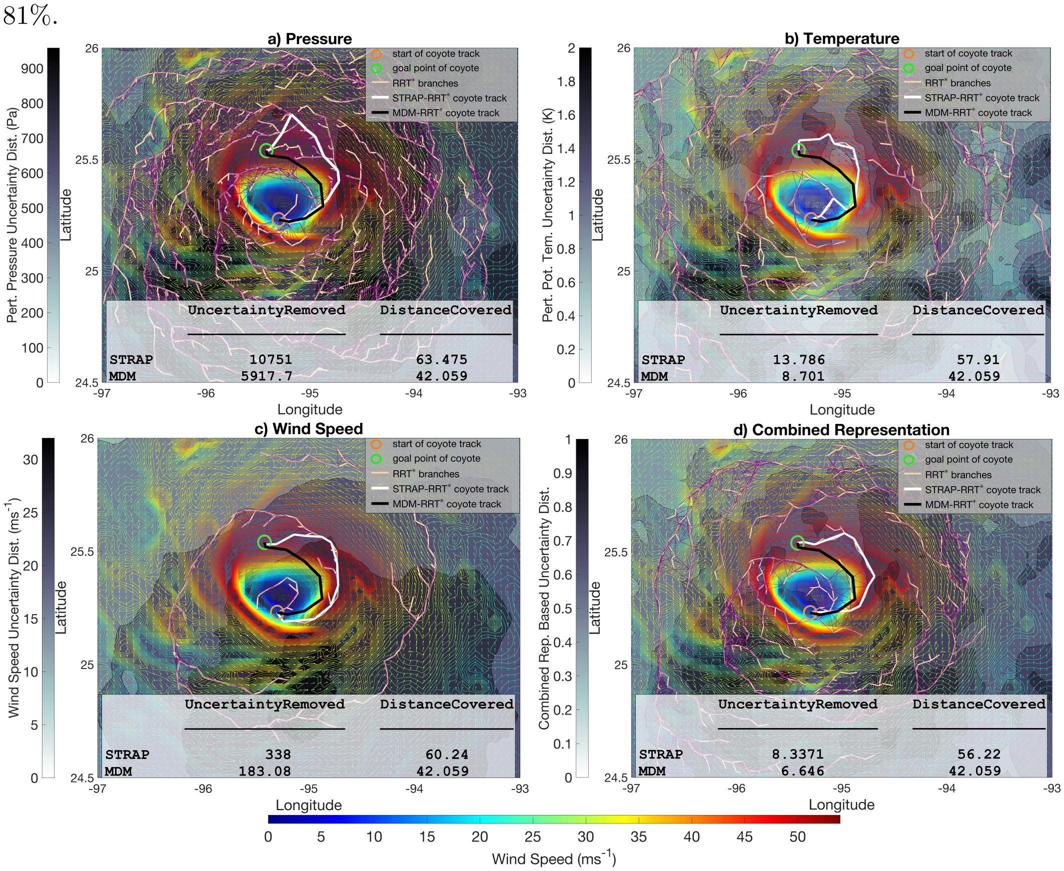

Figure 4. Safe and efficient Coyote path solution at an altitude 1.1 km (ASL) for STRAP-RRT* and MDM layered with uncertainty distribution plots of Hurricane Harvey on 25th August 2017, TIME: 00:00:00.

As expected, the Coyote track distance for STRAP-RRT* was higher than MDM, with track distances 63.47 miles and 42.26 miles respectively, corresponding to a 50% increase in distance for Coyote using STRAP-RRT*. The findings in Figure 4b show significant potential in improving observation of temperature using STRAP-RRT*. When compared to MDM, there is an increase in total uncertainty removed from 8 K to 13 K, representing an improvement of over 58%. The increase in total uncertainty removed occurred at a 37% increase in Coyote track distance for STRAP-RRT*. The findings in Figure 4c show that STRAP-RRT* preformed better than MDM in removing wind speed uncertainty. Improvement in wind speed uncertainty removal from 183 ms^{-1} to 338 ms^{-1} is observed for STRAP-RRT* compared to MDM, representing a 84% increase. The Coyote track distance for STRAP-RRT* and MDM are 60 miles and 42 miles respectively, corresponding to a 43% increase in Coyote track distance using STRAP-RRT*. STRAP-RRT* on the combined representation for uncertainty distribution (Figure 4d) reported improvements of over 25% when compared to the MDM. This occurs at a 40% increase in Coyote sUAS track distance to the goal location. Overall, the performance of the model on individual uncertainty distribution tends to be similar to that of the combined representation. The trade-off between total uncertainty removed and the total distance is reasonable, considering the algorithm allows the Coyote to minimize the energy utilized and increase range for navigation by using the wind velocity constraint.

4.3 Model Robustness Analysis

To assess the robustness of STRAP-RRT* and MDM, 100 scenarios of start and goal locations are drawn from a uniform sample of locations around the eye region (Figure 5). The following notations identify the implementation results for each state variable: Pressure-STRAP (P_STRAP), Pressure-MDM (P_MDM), Temperature-STRAP (T_STRAP), Temperature-MDM (T_MDM), Wind speed-STRAP (W_STRAP), Wind speed-MDM (W_MDM), Combined representation-STRAP (C_STRAP), and Combined representation-MDM (C_MDM).

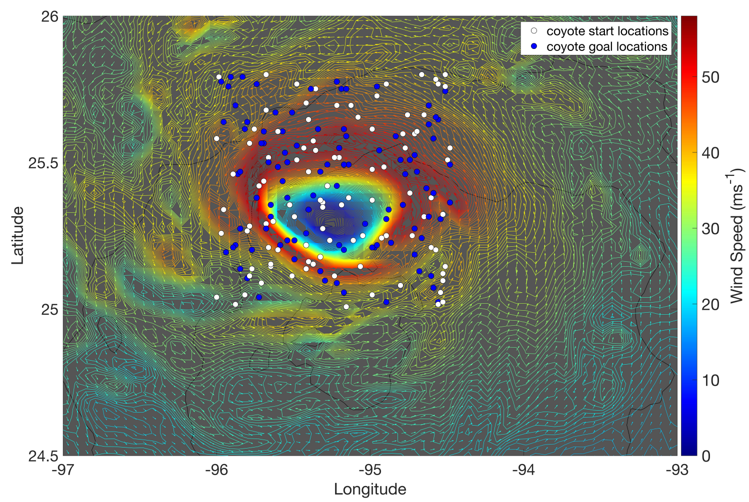

Figure 5. Distribution of 100 randomly sampled flight start and goal locations.

The results of path solution (STRAP and MDM) for each scenario (flight number) is reported considering the same number of observation points. Figure 6 shows the performance of STRAP-RRT* compared to MDM on pressure uncertainty. Percentage increase is calculated as the change in computed value (total uncertainty and distance covered) for STRAP-RRT* relative to MDM. In general, the results indicate good performance for STRAP-RRT* in removing uncertainties, with improvements mostly ranging between 5% and 100%. We mostly observe an increased Coyote track distance for STRAP-RRT* compared to MDM, ranging between 10% and 80%, although a few scenarios of STRAP-RRT* reported decreased flight distance than MDM.

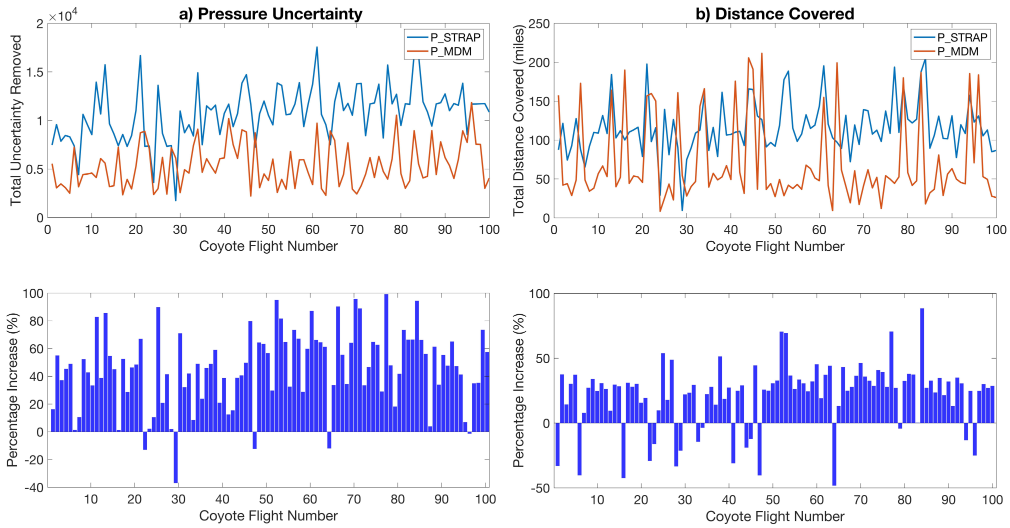

Figure 6. Pressure uncertainty analysis for P_STRAP and P_MDM.

Figure 7 shows the performance of STRAP-RRT* compared to MDM on temperature uncertainty. In most instances, it is seen that STRAP-RRT* resulted in significant improvement in removing uncertainty, with improvements ranging between 5% and 60%. STRAP-RRT* mostly resulted in increased Coyote track distances, although few scenarios reported lower track distances than MDM. A few of these scenarios still resulted in higher uncertainty removal than MDM. Overall, the increased Coyote track distance for STRAP-RRT* ranged between of 1% and 60%.

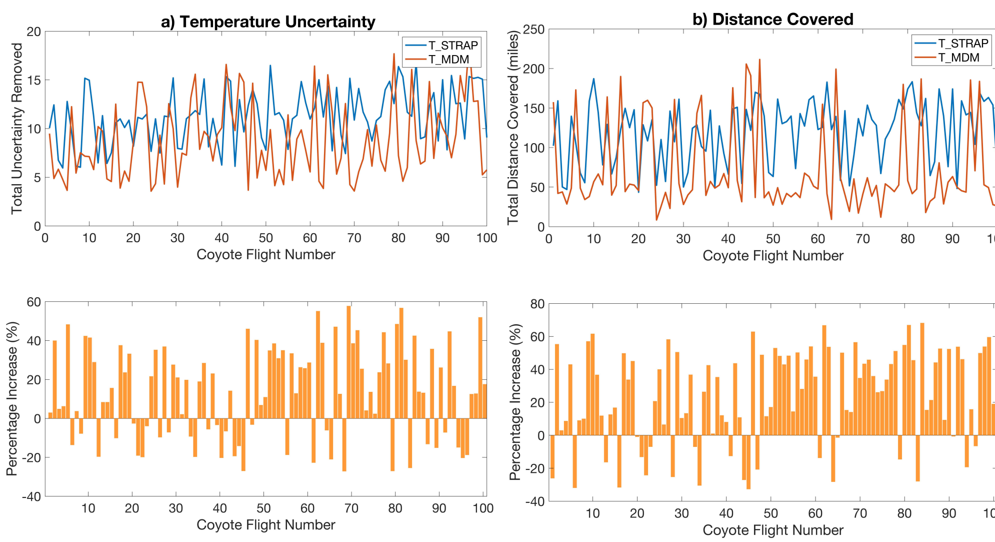

Figure 7. Temperature uncertainty analysis for T_STRAP and T_MDM.

Figure 8 shows the performance of STRAP-RRT* compared to MDM on wind speed uncertainty. STRAP-RRT* results indicate a similar trend of good performance as seen above for pressure (Figure 6), although a few scenarios reported lower improvement levels. Improvement in uncertainty removal ranged between 2% and 60%. Although multiple scenarios reported a lower track distances for STRAP-RRT* than MDM, a few of thee scenarios reported a higher uncertainty removal than MDM. Increases in Coyote track distance for STRAP-RRT* ranged between 1% and 62%.

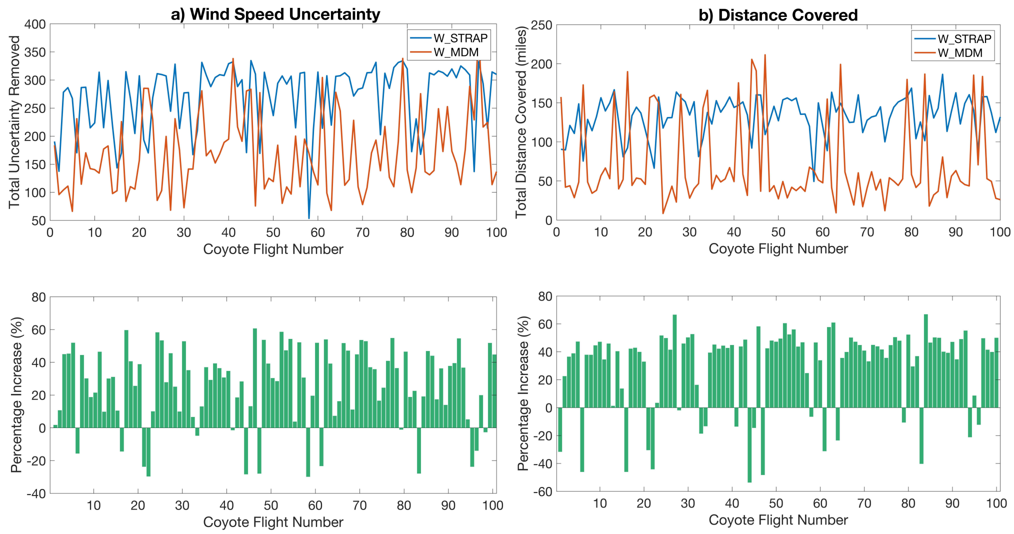

Figure 8. Wind speed uncertainty analysis for W_STRAP and W_MDM.

Figure 9 shows the performance of STRAP-RRT* compared to MDM on the combined representation for uncertainty. Clearly, STRAP-RRT* results in significant improvements in the removal of uncertainty, with improvements mostly ranging between 5% and 75%. A few scenarios resulted in lower track distances for STRAP-RRT* than MDM, although a number these scenarios reported a higher uncertainty removal than MDM. The increased Coyote track distance for STRAP-RRT* ranged between 1% and 90%.

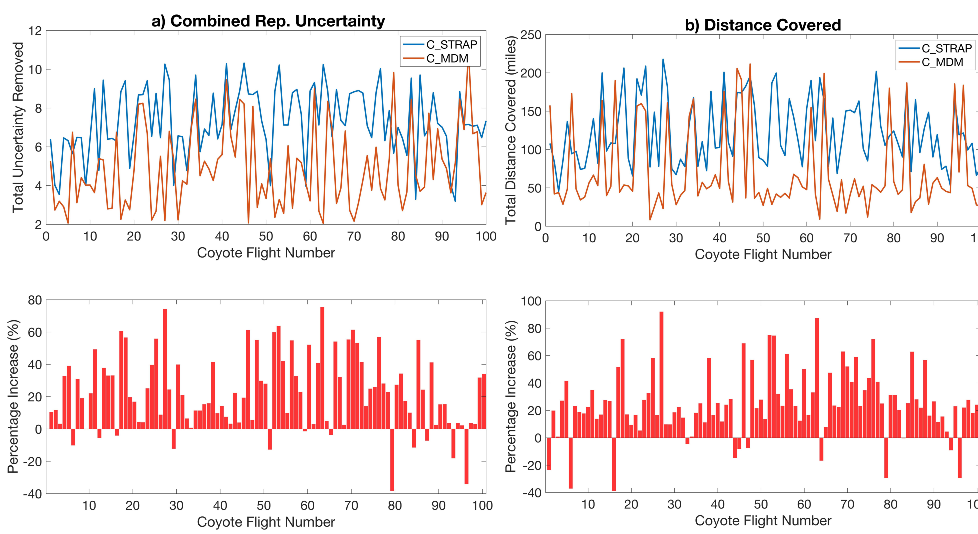

Figure 9. Combined representation uncertainty analysis for C_STRAP and C_MDM.

The parallel boxplots in Figure 10 illustrate the distribution of uncertainty removal and distance covered for the different observations of state variables for STRAP-RRT* and MDM. STRAP-RRT* distribution indicated good performance for uncertainty removal with few outlier values. Interquartile ranges for uncertainty removal using STRAP-RRT* are typically higher than MDM. In all cases of uncertainty removal analysis, STRAP-RRT* reported a higher median than MDM. The uncertainty removal distribution for pressure (P_STRAP) had the highest number of outliers, while T_STRAP, T_MDM, C_MDM and C_STRAP reported no outliers.

The distribution of total distance covered is as expected. Interquartile ranges for STRAP-RRT* are typically larger than MDM, indicating a higher overall track distance. The distribution of Coyote sUAS flight distance considering pressure observation (P_STRAP) has the highest number of outliers. Overall, the mean flight distance for Coyote flights using STRAP-RRT* was greater than MDM.

The findings of the Monte-Carlo simulation suggest good performance for STRAP-RRT* in targeting locations of high uncertainties. This determination is mostly due in part to STRAP-RRT* evaluating the background uncertainty in deciding which location to visit. The implementation of STRAP-RRT* on the combined representation showed excellent performance, reporting no outliers for total uncertainties removed and distance covered.

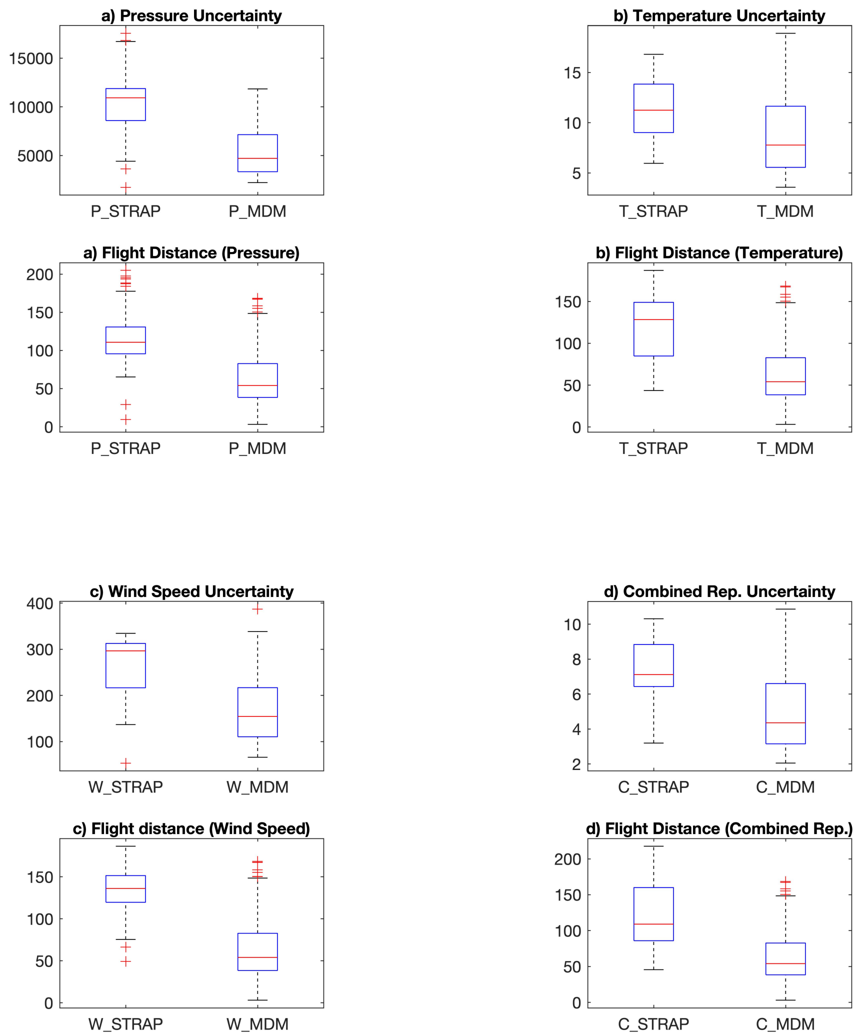

Figure 10. Summary statistics for flight total uncertainty removed and flight distance analysis.

This performance is especially significant since observations of the different state variables are made simultaneously as the Coyote sUAS traverses a given path and therefore the actual benefit of STRAP-RRT* can be truly deduced from the analysis of the combined representation for uncertainty distribution. A significant resolution of uncertainties at the inner-core can therefore be achieved using STRAP-RRT*, which will result in an improved estimation of the inner-core structure.

5 Data Assimilation

The relative significance in improvement achieved by removing uncertainty can be assessed through a data assimilation analysis. Data assimilation adjusts state variables (temperature, pressure, and wind speed) directly during a period for which you want estimates of the state variables. We perform preliminary data assimilation analysis equivalent to a simple scalar illustration of the least-squares estimation for a typical flight mission using STRAP-RRT*.

5.1 Merging Coyote sUAS Observations and Prior Model Data

The series of discrete point in situ observations by the Coyote sUAS is assimilated with the prior estimates of the TC to provide the best estimate (posterior) of the TC structure. The model state estimate is assumed to be univariate and represented as grid-point values. Assume two observations given by:

model background information at location i:

$$M_{model(i)} + \sigma^2_{model(i)}, \tag{7}$$

and after Coyote sUAS observation at location i:

$$M_{obs(i)} + \sigma^2_{obs(i)}. \tag{8}$$

In a scenario where observations are treated as excellent, the data assimilation method will replace the model data at the location with the observation. Observations are far from perfect; therefore, assimilation is usually carried out through a weighted estimate of model and observation based on their respective uncertainty. The best estimate at location i is written as:

$$\textbf{Best estimate}_{(i)} = (1-\beta)M_{model(i)} + \beta M_{obs(i)}. \tag{9}$$

β is the weight between the model and observation. The best estimate of weight considers the uncertainty of simulation model and observation, written as:

$$\beta = \frac{\sigma^2_{model(i)}}{\sigma^2_{model(i)} + \sigma^2_{obs(i)}}. \tag{10}$$

The uncertainty (error variance) of the best estimate is less than the uncertainty of either the model or the observation written as:

$$\sigma^2_{\textbf{best estimate}(i)} = (1-\beta)\sigma^2_{model(i)}. \tag{11}$$

To account for the effect of an influence region around each observation point, we introduce a weighting function $w(i,j)$ to update the best estimates of the uncertainty at each grid locations j in the vicinity of observation point i written as:

$$w(i,j) = \max\left(0, \frac{R^2 - d^2_{i,j}}{R^2 + d^2_{i,j}}\right) \tag{12}$$

where $d_{i,j}$ is a measure of the distance between points i and j. The weighting function $w(i,j)$ equals to one if the grid point j is collocated with observation i. It is a deceasing function of distance which is zero if $d_{i,j} \geq R$. R ("the influence region or radius") is a user defined constant beyond which the observations have no weight. In this analysis, we assume β from Equation 10 is directly related to the accuracy of the instrument making the observation. The modified best estimate of the uncertainty at each grid point location j can now be written as:

$$\sigma^2_{\textbf{best estimate}(j)} = (1-\beta * w(i,j))\sigma^2_{model(j)}. \tag{13}$$

5.2 Data Assimilation Analysis

This section's focus is to illustrate the resulting improvements from a typical Coyote sUAS mission in a TC using the proposed deployment scheme. The analysis is carried out using the combined representation for uncertainty distribution. Although spatial correlation is not considered, we still show promising improvements. Future research is expected to have more benefits from correlation gains. A typical data assimilation process without considering the spatial correlation is shown in Figure 11. Note that uncertainty distribution values along the recommended path of the Coyote sUAS are almost reduced to zero. We assume an influence region $R = 6$ miles around each observation point. The mission starts with a fixed drop-off location at 25.5495^o N, 94.3398^o W and a randomly sampled without replacement multiple-goal locations. To ensure the utilization of all Coyote's endurance during a flight, we report the results for missions with total distance in the range of $60 \leq$ distance ≤ 105. The goal location of a previous flight is set to be the start location of the next flight. After Coyote finds a goal location, we update the uncertainty distribution to reflect the new distribution resulting from our previous observation. We assume a uniformly distributed β between 0.8 and 0.9 (given that observations are at least 80% more important than the simulation model but less than 90% important than the simulation model) at different locations in the TC space.

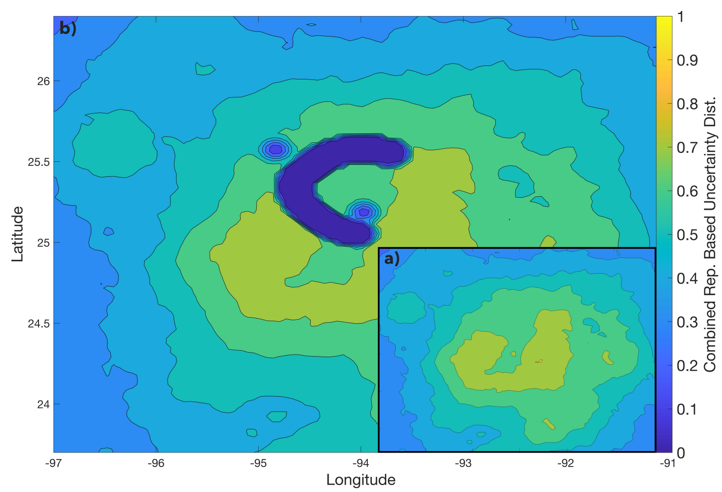

Figure 11. Illustration of a data assimilation process after Coyote flight mission using STRAP-RRT* a) Before assimilation of Coyote flight data, b) After assimilation of Coyote flight data.

Table 2 shows the results of improvement in the estimates of the TC structure. Improvement in TC estimates is calculated as the difference between the sum of TC error variances before data assimilation (Figure 11a) and the sum of TC error variances after Coyote flight data assimilation (Figure 11b). State variables pressure and wind speed reported a relatively high and similar trend in improvements. This can mainly be due to the similarities in the uncertainty distribution for these two state variables. Temperature reported the lowest percentage improvement, mainly due to the very sparse distribution of uncertainty. Note that the results are the improvements for the entire TC structure, and thus represents an underestimate of actual improvement for the inner-core region.

Table 2. Summary of percentage improvement in simulation model for Hurricane Harvey after data assimilation using STRAP-RRT*

	Destination		% Improvement		
Distance Covered (miles)	Latitude	Longitude	Pressure	Temperature	Wind Speed
65.7312	25.7677	-94.9002	2.2747	0.8587	1.6967
81.9842	25.0242	-94.5855	3.6507	1.3229	2.9478
86.9840	25.2747	-94.5087	3.4549	1.2578	2.7544
99.0933	25.0646	-94.6238	3.5981	1.3006	2.9096
102.9406	25.1939	-94.6238	3.4407	1.2513	2.7442

In general, the analysis indicates the Coyote sUAS mission with goal destination 25.0242^o N, 94.5855^o W would have resulted in the most improvement in the estimates of the TC structure although the distance covered in this mission is relatively smaller when compared to the last three mission in Table 2.

6 conclusion

This study presents a sampling-based path planning algorithm to optimize the use of sUAS for useful data collection in TCs. In order to minimize the energy utilized for navigation, a directional constraint is implemented as an acceptable angular difference between a sub-path segment and the wind velocity allowing the sUAS to mostly follow the strong TCs wind direction. The current study highlights a promising solution for sUAV navigation as they can fly into the targeted TC inner core to obtain high-resolution meteorological observations guided by background estimates (e.g., ensemble spread and sensitivity map) from an earlier data assimilation process. The new observations from the TC boundary layer (i.e., interface between the ocean and atmosphere) supplement existing partial knowledge (Cione et al., 2013) for a better estimate of TC intensity. Although we did not consider the spatial correlation in the TC structure, the results showed significant improvement in the accuracy of the TC structure after Coyote sUAS followed the recommended path from STRAP-RRT*.

In future research, a systematic investigation using a sensitivity map will be considered, incorporating the storm structure's spatiotemporal dependencies. A sensitivity map indicates how much each location affects the improvement of the inner-core initialization. We will also consider an extension to a multiagent collaborative framework. Past TC missions have deployed multiple Coyote sUAS one at a time independently with only a limited area of coverage or point measurement. However, this scheme makes the monitoring difficult for different sections of the boundary layer, failing to utilize the collaborative framework. A previous decision of first location assignment of the Coyote sUAS could turn out to be not optimal, after computing the expected benefit of the second assignment of the Coyote sUAS. On the contrary, poor information gathered as a result of the first location assignment could have a cascading effect on the following Coyote sUAS assignments. A myopic decision may focus more on information gain on the one Coyote sUAS assignment in the current stage, but if the next assignment location is too far, a relatively late arrival time could lower the chance of collecting critical data in the second stage since the TC has already moved.

Acknowledgments
Funding for this research was provided by NASA JPL RSA #1646362 and NSF RI #1910397. Additional partial support was provided by the NASA JPL Education office. The authors also express thanks to all editors and reviewers of this article. The data used for these analyses are available at: `https://figshare.com/s/90f31f60e5821dae90bd`

References

Cione, J. J., Bryan, G. H., Dobosy, R., Zhang, J. A., de Boer, G., Aksoy, A., ... others (2020). Eye of the storm: observing hurricanes with a small unmanned aircraft system. *Bulletin of the American Meteorological Society*, *101*(2), E186–E205.

Cione, J. J., Kalina, E., Uhlhorn, E., Farber, A., & Damiano, B. (2016). Coyote unmanned aircraft system observations in hurricane edouard (2014). *Earth and Space Science*, *3*(9), 370–380.

Cione, J. J., Kalina, E. A., Zhang, J. A., & Uhlhorn, E. W. (2013). Observations of air–sea interaction and intensity change in hurricanes. *Monthly Weather Review*, *141*(7), 2368–2382.

de Boer, G., Argrow, B., Cassano, J., Cione, J., Frew, E., Lawrence, D., ... Wolff, C.

(2019). Advancing unmanned aerial capabilities for atmospheric research. *Bulletin of the American Meteorological Society*, *100*(3), ES105–ES108.

DeMaria, M., & Kaplan, J. (1999). An updated statistical hurricane intensity prediction scheme (ships) for the atlantic and eastern north pacific basins. *Weather and Forecasting*, *14*(3), 326–337.

DeMaria, M., Mainelli, M., Shay, L. K., Knaff, J. A., & Kaplan, J. (2005). Further improvements to the statistical hurricane intensity prediction scheme (ships). *Weather and Forecasting*, *20*(4), 531–543.

DeMaria, M., Sampson, C. R., Knaff, J. A., & Musgrave, K. D. (2014). Is tropical cyclone intensity guidance improving? *Bulletin of the American Meteorological Society*, *95*(3), 387–398.

Goyal, P. K., & Datta, T. (2011). Probability distributions for cyclone key parameters and cyclonic wind speed for the east coast of indian region. *The International Journal of Ocean and Climate Systems*, *2*(3), 209–223.

Malakar, P., Kesarkar, A. P., Bhate, J., & Deshamukhya, A. (2020). Appraisal of data assimilation techniques for dynamical downscaling of the structure and intensity of tropical cyclones. *Earth and Space Science*, *7*(2), e2019EA000945.

Minamide, M., Zhang, F., & E, C. E. (2020). Nonlinear forecast error growth of rapidly intensifying hurricane harvey (2017) examined through convection-permitting ensemble assimilation of goes-16 all-sky radiances. *Journal of the Atmospheric Sciences*.

Munsell, E. B., Zhang, F., & Stern, D. P. (2013). Predictability and dynamics of a nonintensifying tropical storm: Erika (2009). *Journal of the Atmospheric Sciences*, *70*(8), 2505–2524.

Pillar-Little, G. B. R., Elizabeth A, Lappin, F. M., Bell, T. M., Segales, A. R., de Azevedo, G. B. H., Doyle, W., ... Chilson, P. B. (2020). Observations of the thermodynamic and kinematic state of the atmospheric boundary layer over the san luis valley, co using remotely piloted aircraft systems during the lapse-rate field campaign. *Earth System Science Data Discussions*, 1–17.

Raavi, P. H., & Walsh, K. (2020). Sensitivity of tropical cyclone formation to resolution-dependent and independent tracking schemes in high-resolution climate model simulations. *Earth and Space Science*, *7*(3), e2019EA000906.

Rosendal, H. E., & Shaw, S. L. (1982). Relationship of maximum sustained winds to minimum sea level pressure in central north pacific tropical cyclones.

Sanabia, E. R., Barrett, B. S., Black, P. G., Chen, S., & Cummings, J. A. (2013). Real-time upper-ocean temperature observations from aircraft during operational hurricane reconnaissance missions: Axbt demonstration project year one results. *Weather and Forecasting*, *28*(6), 1404–1422.

Shea, D. J., & Gray, W. M. (1973). The hurricane's inner core region. i. symmetric and asymmetric structure. *Journal of the Atmospheric Sciences*, *30*(8), 1544–1564.

Sippel, J. A., & Zhang, F. (2008). A probabilistic analysis of the dynamics and predictability of tropical cyclogenesis. *Journal of the Atmospheric Sciences*, *65*(11), 3440–3459.

Sippel, J. A., & Zhang, F. (2010). Factors affecting the predictability of hurricane humberto (2007). *Journal of the Atmospheric Sciences*, *67*(6), 1759–1778.

Stern, D. P., Bryan, G. H., & Aberson, S. D. (2016). Extreme low-level updrafts and wind speeds measured by dropsondes in tropical cyclones. *Monthly Weather Review*, *144*(6), 2177–2204.

Tyrrell, G., & Holland, G. (2003). Continuous monitoring of the hurricane core: Availability of new long-endurance small drone aircraft. *Hurricane! Coping with Disaster: Progress and Challenges Since Galveston, 1900*, *55*, 291–304.

Van Sang, N., Smith, R. K., & Montgomery, M. T. (2008). Tropical-cyclone intensification and predictability in three dimensions. *Quarterly Journal of the Royal Meteorological Society: A journal of the atmospheric sciences, applied meteorology and physical oceanography*, *134*(632), 563–582.

Wu, Y., Shen, Z., & Tang, Y. (2020). A flow-dependent targeted observation method for ensemble kalman filter assimilation systems. *Earth and Space Science*, e2020EA001149.

Zhang, F., Minamide, M., Nystrom, R. G., Chen, X., Lin, S.-J., & Harris, L. M. (2019). Improving harvey forecasts with next-generation weather satellites: Advanced hurricane analysis and prediction with assimilation of goes-r all-sky radiances. *Bulletin of the American Meteorological Society*, *100*(7), 1217–1222.

Zhang, J. A., Cione, J. J., Kalina, E. A., Uhlhorn, E. W., Hock, T., & Smith, J. A. (2017). Observations of infrared sea surface temperature and air–sea interaction in hurricane edouard (2014) using gps dropsondes. *Journal of Atmospheric and Oceanic Technology*, *34*(6), 1333–1349.